AIChE

Chemical Kinetic Modeling of i-Butane and n-Butane Catalytic Cracking Reactions over HZSM-5 Zeolite

Gholamreza Roohollahi and Mohammad Kazemeini
Dept. of Chemical and Petroleum Engineering, Sharif University of Technology, Tehran, Iran

Alireza Mohammadrezaee and Reza Golhosseini
Petrochemical Research and Technology Company, National Petrochemical Company, Tehran, Iran

DOI 10.1002/aic.12750
Published online October 19, 2011 in Wiley Online Library (wileyonlinelibrary.com).

A chemical kinetic model for i-*butane and* n-*butane catalytic cracking over synthesized HZSM-5 zeolite, with SiO_2/Al_2O_3 484, and in a plug flow reactor under various operating conditions, has been developed. To estimate the kinetic parameters of catalytic cracking reactions of* i-*butane and* n-*butane, a lump kinetic model consisting of six reaction steps and five lumped components is proposed. This kinetic model is based on mechanistic aspects of catalytic cracking of paraffins into olefins. Furthermore, our model takes into account the effects of both protolytic and bimolecular mechanisms. The Levenberg–Marquardt algorithm was used to estimate kinetic parameters. Results from statistical F-tests indicate that the kinetic models and the proposed model predictions are in satisfactory agreement with the experimental data obtained for both paraffin reactants.* © 2011 American Institute of Chemical Engineers *AIChE J*, 58: 2456–2465, 2012
Keywords: i-butane, n-butane, kinetic model, HZSM-5, catalytic cracking

Introduction

Analysis and optimization of the catalytic processes involved in transformation of light paraffins into more desirable light olefins, especially propylene, is a growing field of research.[1–4] Differences in market prices between light paraffins and olefins, coupled with the high-energy requirements of noncatalytic steam cracking reactions with low propylene yields (which currently supply 67% of total propylene production), have made catalytic processes for the production of light olefins more attractive.[5,6] Thus, determination of the reaction mechanisms behind these catalytic processes is an important area of research. Transformation of paraffins over ZSM-5 catalysts proceeds via two well-known mechanisms: (1) the protolytic (monomolecular) mechanism, which results in the formation of smaller olefins and paraffins through protolytic cracking reactions and (2) the classical bimolecular carbenium ion mechanism, which transforms paraffins into their corresponding olefin via hydrogen transfer reactions.[7–17] The protolytic mechanism is favored at high reaction temperatures, low partial pressures of paraffin, and low conversions. Moreover, with decreasing aluminum content in the zeolite structure, the relative contribution of the protolytic mechanism increases vs. the bimolecular mechanism.[9]

HZSM-5 is a medium pore size zeolite that reduces the occurrence of the bimolecular mechanism in favor of the protolytic mechanism due to steric constraints associated with the formation of bimolecular transition states of the classical chain mechanism and a lack of space near acidic sites.[7,8,14] This type of zeolite also enhances protolytic cracking reactions over secondary reactions because of its special shape selectivity, moderate acidic strength, and low capacity for hydrogen transfer.[2] Catalytic cracking of *n*-butane and *i*-butane, two light paraffins, results in a simple product distribution that uses only a single type of carbonium ion as a reaction intermediate, which is formed by protonation over a zeolite catalyst. Moreover, catalytic cracking of these two alkanes mainly produces light olefins, particularly propylene, in high yield, with a low selectivity toward heavy products. Hence, many authors have investigated the mechanism and kinetics behind the catalytic cracking of butanes.[13–20]

Kinetic modeling is a very useful tool to develop a better understanding of catalytic cracking reactions. Several authors have investigated the kinetics of paraffin catalytic cracking over HZSM-5 zeolite catalysts, using microkinetic modeling.[21–26] However, one of the problems associated with detailed models, such as the microkinetic model, is the large number of individual reaction steps involved, each with its own rate constant that must be estimated. In addition, because of the low number of carbon atoms in butanes, catalytic cracking reactions for these paraffins are not complex enough to require a detailed microkinetic model, which is more appropriate for heavier paraffins. Recently, a lumped kinetic model was proposed to predict the behavior of *n*-butane cracking over HZSM-5; a model consisting of a seven-step kinetic scheme with five lump compounds properly predicted the product distribution.[2]

The objective of the present study was to present a simple lumped kinetic model takes into account the effects of both protolytic and bimolecular mechanisms, which suitably describes the dependency of products yield on process

Correspondence concerning this article should be addressed to M. Kazemeini at kazemini@sharif.edu.

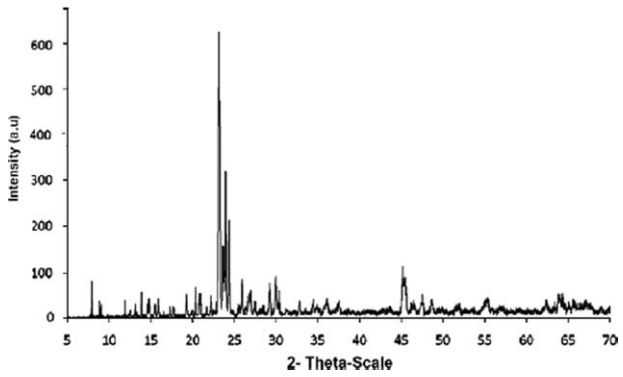

Figure 1. X-ray diffraction pattern of the HZSM-5 zeolite sample.

variables for catalytic cracking of *n*-butane and *i*-butane. Although previous studies have been reported for *i*-C_4 and *n*-C_4 cracking, to the best of our knowledge, this is the first report on the kinetic modeling of isobutane catalytic cracking over HZSM-5 zeolite. The present work aimed at determining a kinetic model that allows quantifying product distribution by focusing on the light olefins in particular; C_2^{2-}–C_4^{2-}. Several experiments conducted on HZSM-5 zeolites using different Si/Al ratios, and the zeolite sample used in the present study (with a Si/Al ratio = 484) displayed the highest selectivity toward light olefins, coupled with a very low selectivity for heavy products.

Materials and Methods

Catalyst preparation

HZSM-5 zeolite with a SiO_2/Al_2O_3 ratio of 484 was synthesized by the following method: 0.311 g of $NaAlO_2$ (composition: 53 wt % Al_2O_3, 44.5 wt % Na_2O, and 2.5 wt % H_2O) was partially dissolved in 433.6 mL of 0.215 N sodium hydroxide by vigorous stirring, followed by slow addition of 41.078 g of tetra-*n*-propylammonium hydroxide (40 vol %, Merck) as a template. Silicic acid ($SiO_2 \cdot 0.5H_2O$, 54.060 g) was then added to the above mixture under vigorous stirring at ~500 rpm. After ~60 min, the pH of the mixture was adjusted to 10.0 by the addition of ~5 g of 98% sulfuric acid. The resulting mixture had the following composition: 0.775 mol SiO_2, 0.0016 mol Al_2O_3, 0.0485 mol Na_2O, 0.0808 mol $(CH_3CH_2CH_2)_4NOH$, and 25.854 mol H_2O. The mixture was placed in a PTFE lined vessel and heated to 105°C at atmospheric pressure for 12 days under reflux, at a stirring rate of ~100 rpm. The resulting solid product was cooled to room-temperature, removed, and washed with 30 L of H_2O. The product was then dried overnight at 105°C. A portion of the resulting product was subjected to X-ray analysis, which identified the ZSM-5 phase. Ion exchange was performed four times, with 1 M NH_4NO_3 solution at 90°C for 4 h, followed by calcination at 560°C in air for 10 h, to give H-form products. The zeolite powder was pressed using a high-pressure piston for 10 min and then crushed and sieved to a particle diameter between 0.4 and 0.3 mm.

Catalyst characterization

The structures of the above synthesized materials were confirmed to be ZSM-5 zeolite by X-ray diffraction (Figure 1). The BET surface area (S_{BET}) was measured using the N_2 adsorption method (Quantachrome). Before adsorption–desorption measurements, 0.533 g of fresh zeolite sample was degassed at 300°C under N_2 flow for 2 h. The acidity of the sample and the concentration of acid sites on the catalyst surface were measured by temperature-programmed desorption of ammonia (NH_3-TPD, Micromeritics), equipped with an on-line thermal conductivity detector (TCD). The physicochemical properties of the zeolite under investigation are presented in Table 1.

Table 1. Physicochemical Properties of the Zeolite Samples

SiO_2/Al_2O_3 molar ratio	484
Total acidity (mmol of NH_3)g^{-1}	0.199
Surface area ($m^2\ g^{-1}$, S_{BET})	346.223
Total pore volume, V_p ($cm^3\ g^{-1}$)	$0.15 < V_p < 0.4$
Average pore diameter, d_p (nm)	$2 < d_p < 20$
Mean crystallite size, S (μm)	$1 < S < 12$

Scanning electron microscope (SEM) images of the ZSM-5 crystals were acquired using a TESCAN microscope (Model, VEGA). To prepare samples for SEM, a drop of dilute colloidal solution of ZSM-5 was placed onto the SEM sample stud surface and dried at room-temperature. Shortly before SEM image acquisition, the sample was coated with gold. An SEM image of a dried sample is shown in Figure 2. As indicated, the particles have cubiclike morphologies. Average particle sizes for the zeolite sample were estimated based on the SEM images and are reported in Table 1.

Catalyst performance

n-Butane and *i*-butane cracking reactions were performed in a stainless steel tubular fixed-bed reactor with an inner diameter of 10 mm. All runs were performed under a total pressure of 104 kPa and a reactant partial pressure of 20 kPa. This was obtained by accurate mixing of the paraffin with N_2 as a diluent gas, using two MFCs in steady-state flow mode. A schematic diagram of the experimental setup is shown in Figure 3. The reactor was heated and kept under isothermal conditions using a vertical furnace equipped with three electrically heated thermal zones, and maintained at the desired temperature by controlling the internal temperature of the reactor using a TIC and type K thermocouple inserted into the middle of the catalyst bed. Reactions were performed at 470–530°C and a butane space velocity of 0.24–2.65 $g_{C4.}\ (h\ g_{cat})^{-1}$. The length of the reactor was more than adequate to provide the desired temperature for inlet gases before the reaction over

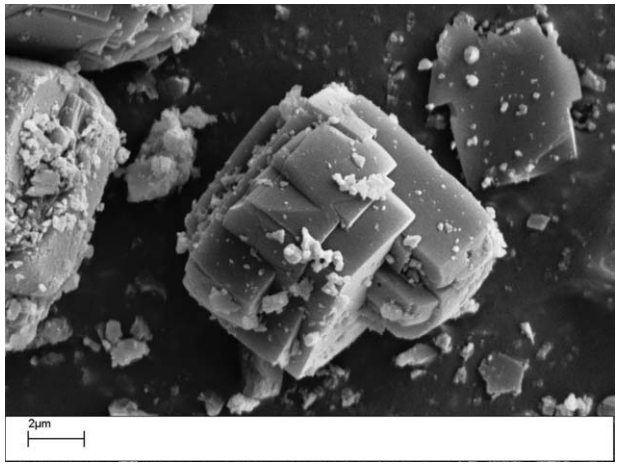

Figure 2. The SEM image of HZSM-5 sample.

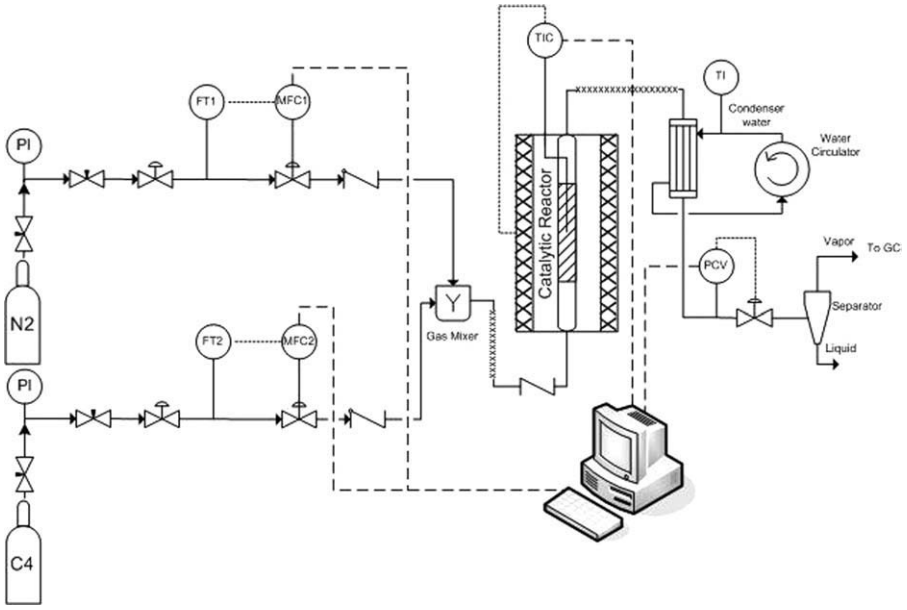

Figure 3. The schematic of the experimental setup.

the catalyst bed. Catalyst (1.00 g) diluted with 1.00 g of quartz was loaded into the reactor.

Product samples were withdrawn periodically at regular intervals from the outlet of the reactor for on-line gas chromatography (GC) analysis. The gas chromatograph (Varian CP, model 4900) was equipped with Star Toolbar software and a TCD, and had four capillary columns for separating heavy C_5–C_7 paraffins, light C_1–C_4 paraffins, C_2–C_7 olefin, CO, CO_2, He, and H_2. Possible heavy products were separated using a decanter and condenser, with the temperature of the cooling side adjusted to 1°C before transferring the products for on-line GC analysis. A small portion of the liquid phase was transferred to the gas chromatograph (Varian CP model 3800), which was equipped with a TCD and FID, and had a capillary column for separating C_7^+ hydrocarbons. For each run, the first sample was analyzed 1 h after the reactant was introduced into the reactor. During a typical run, subsequent GC analyses were conducted at 1 h intervals. Butane conversion and selectivity for all species remained stable during each run.

Catalytic activity tests

Butane conversion, product selectivity, and yield were defined as follows

$$\text{conversion } (\%) = \frac{F_o - F_e}{F_o} \tag{1}$$

$$\text{selectivity i } (\%) = \frac{n_i \times F_{ie}}{4 \times (F_o - F_e)} \tag{2}$$

$$\text{yield i } (\%) = \text{selectivity i} \times \text{conversion} \tag{3}$$

where F_o, F_e, and F_{ie} are the inlet and outlet butane molar flow rates, and the exit molar flow rate of compound i, all in mol h^{-1}, respectively. The selectivity value for each compound i was based on the number of carbon atoms for that compound, n_i (i.e., CH_2 basis). The term "gas hourly space velocity (GHSV)" is the inverse of the contact time and is defined as the mass flow rate of C_4 in g h^{-1} over the total mass of catalyst, i.e.

$$\text{GHSV} = \frac{(F_o)}{W} \qquad \left(\frac{g_{C_4}}{g_{cat}.h}\right) \tag{4}$$

where W is the weight of the catalyst in grams. GHSV values were wide ranging from 0.24 to 2.65 h^{-1}.

n-Butane cracking

Products in the present study were classified based on type and carbon number into the following lumps: (1) olefins, ethylene, propylene, and butene; (2) paraffins, ethane, propane, and butane; (3) heavy products, olefin, and paraffins with five or more carbons, and (4) methane. Figure 4 shows the product selectivity for *n*-butane cracking at 530°C as a function of GHSV. As can be seen, an increase in GHSV led to lower *n*-butane conversion. In addition, the selectivity for light olefins was enhanced, whereas the selectivity for light paraffins was lowered. Furthermore, the selectivity for methane remained relatively unchanged, whereas the

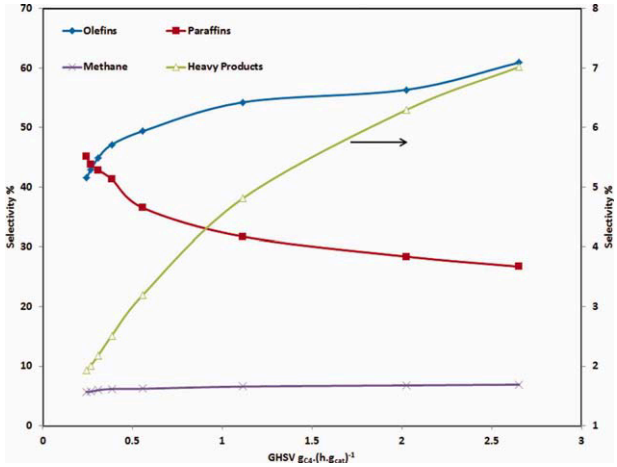

Figure 4. Effect of GHSV on product distributions from *n*-butane cracking at 530°C.

[Color figure can be viewed in the online issue, which is available at wileyonlinelibrary.com.]

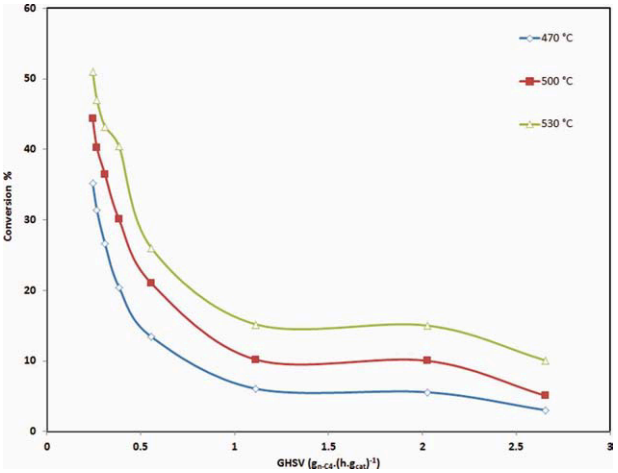

Figure 5. Effect of GHSV on *n*-butane conversion at different temperatures.

[Color figure can be viewed in the online issue, which is available at wileyonlinelibrary.com.]

selectivity for heavy products significantly increased with increasing GHSV.

The variation in *n*-butane conversion as a function of GHSV at three different temperatures is presented in Figure 5, which demonstrates that the decrease in *n*-butane conversion with increasing GHSV is more significant at higher temperatures. Figure 6 shows the variation in light olefin yield as a function of contact time at three reaction temperatures. The contact time, τ, is defined as the inverse of the GHSV value

$$\tau = \frac{1}{\text{GHSV}} \qquad \left(\frac{(g_{cat}.h)}{g_{C_4}}\right) \tag{5}$$

Although the selectivity for light olefins is increased with increased GHSV, light olefin yields were decreased with decreased contact time due to a decrease in *n*-butane conversion with increasing GHSV.

On the basis of the above experimental observed behaviors and the use of the monomolecular and bimolecular mechanisms in this study, one may conclude that results of this research are indeed consistent with those of Haag and Dessau.[7] In other words, these observations were in agreement with the mechanistic interpretation of Haag and Dessau. Products yield and *n*-butane conversion remained relatively constant and stable with time-on-stream, indicating that the zeolite used in this investigation catalyzed *n*-butane cracking with minimal coke formation; and, thus, minimal catalyst deactivation. Stable performance was even observed at low GHSV values and high temperatures. Figure 7 shows the evolution of products selectivity and feed conversion with time-on-stream at 530°C, at an *n*-butane partial pressure of 20 kPa and GHSV = 0.24 h^{-1}. Similar data at 470°C were obtained, reported as the supplementary data and might be obtained from the *AIChE Journal*.

i-*Butane cracking*

Catalytic cracking of *i*-butane was also conducted at three temperatures and GHSV values up to 2.03 $g_{i\text{-}C4.}$ $(h\ g_{cat})^{-1}$. The partial pressure of *i*-butane and total pressure were 20 and 104 kPa, respectively. Figure 8 shows the product selectivity for *i*-butane cracking at 530°C as a function of GHSV. Selectivity toward propylene was significantly higher from catalytic cracking of *i*-butane vs. *n*-butane, whereas selectivity for ethane was substantially decreased. Moreover, in contrast to *n*-butane cracking, selectivity toward heavy products from *i*-butane cracking decreased with increasing GHSV.

Figure 9 shows the variation in *i*-butane conversion as a function of GHSV at different temperatures. Figure 10 illustrates the variation in the yield of various light olefins with contact time at 530°C. As can be seen, increased *i*-butane contact time is associated with a significant enhancement in the yield of light olefins, especially propylene and ethylene. In addition, the yield of total light olefins also increased with increasing reaction temperature. One major difference in the distribution of products from *i*-butane catalytic cracking vs. *n*-butane is the significantly higher yields of light olefins (in particular of propylene) for *i*-butane at the expense of light paraffins. Similar to *n*-butane, after 6 h, the evolution of *i*-butane conversions with time-on-stream remained steady, indicating that catalyst deactivation was not significant. However, the coke content of the spent catalyst from *i*-butane was slightly higher than that from *n*-butane cracking.

It is well-known that the yield is the product of conversion and selectivity and as conversion by itself usually increased with temperature, consistent with the findings of Haag and co-workers,[7,12] the selectivity also increased with temperature. This latter findings of Haag and co-workers are also emphasized in Figures 4 and 8 of the present work for *n*-butane and *i*-butane; respectively. Furthermore, the yield of light olefins according to the work of Haag and colleagues should increase with temperature, which is indeed what has been shown in Figures 6 and 11 in this article as well. These results all are indicative of the consistency between the present investigation and that of Haag and co-workers as well as other researchers following their paths.[8–11,13–17]

Similar to *n*-butane, the catalyst deactivation rate for *i*-butane cracking occurred slowly, even at low GHSV values and high temperatures. The attenuation of conversion after nearly 3 h was low for all runs. Figure 12 shows the evolution of the compound conversion and selectivity as a function of time-on-stream for 3 h at 530°C at GHSV = 0.31 $g_{i\text{-}}$

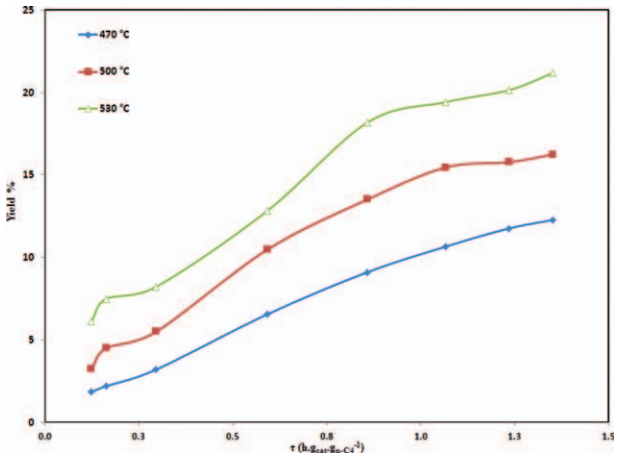

Figure 6. Effect of contact time on light olefin yields from *n*-butane cracking at different temperatures.

[Color figure can be viewed in the online issue, which is available at wileyonlinelibrary.com.]

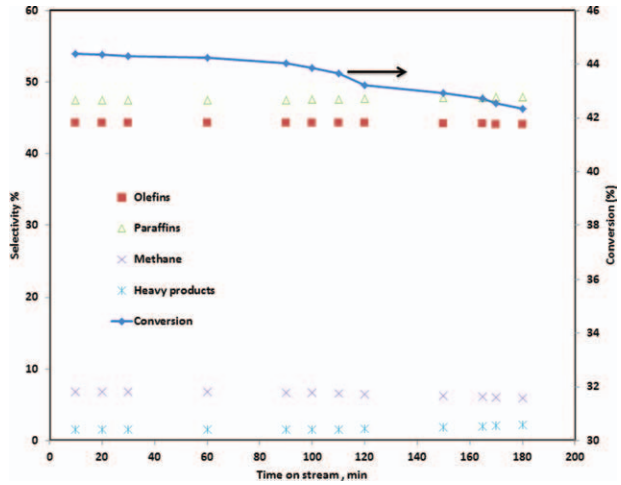

Figure 7. Evolution of product selectivity (left axis) and feed conversion (right axis), $P_{n\text{-}C_4}$ = 20 kPa, GHSV = 0.24 h^{-1}, at T = 530°C.

[Color figure can be viewed in the online issue, which is available at wileyonlinelibrary.com.]

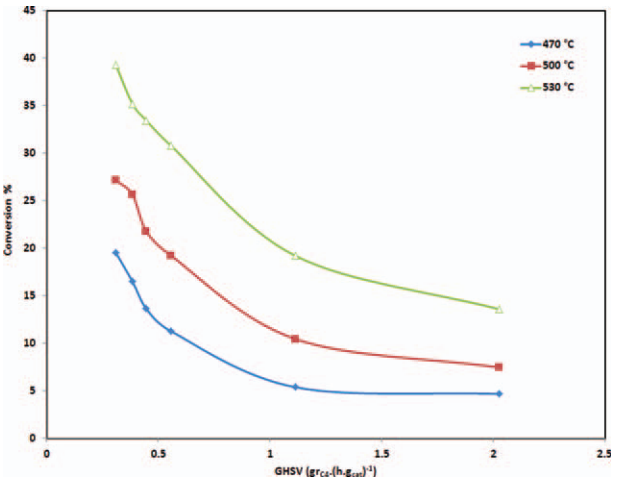

Figure 9. Effect of GHSV on *i*-butane conversion at different temperatures.

[Color figure can be viewed in the online issue, which is available at wileyonlinelibrary.com.]

$_{Cr}$ (h g_{cat})$^{-1}$. The apparent trend at the lowest GHSV values, for which the largest amount of heavy products were produced, indicate that catalyst activity remained steady even at high temperatures. Similar data at 470°C were obtained, reported as the supplementary data and might be obtained from the *AIChE Journal*.

Proposed Kinetic Model

The main objective of this study was to develop a kinetic model with a reasonably low number of reaction steps and kinetic parameters, but which is precise enough to enable a quantitative description and analysis of the key features of *i*-butane and *n*-butane cracking reactions. Instead of creating a detailed kinetic model containing all individual compounds and possible reaction steps in butane cracking, we analyzed several kinetic schemes used in previous studies by incorporating the reaction conditions and product distributions of the current study. A simple kinetic scheme was developed based on five lump components, which showed the highest precision (see Figure 13). This kinetic scheme includes six reaction steps that represent the major reaction pathways during butane cracking reactions, including cracking of butane into light olefins, methane, paraffins, and heavy products, as well as intermediate olefins, and transformation into heavy products and paraffins.

The presented scheme considered both monomolecular and bimolecular mechanisms that occurred simultaneously. Bimolecular mechanism involved the production of heavy components and some of paraffins-like propane, as indicated by Reactions 2, 4, 5, and 6. On the other hand, monomolecular mechanism involved the formation of light components such as light olefins including ethylene, propylene, and methane, as depicted by Reactions 1 and 3.

Furthermore, it should also be noted that the product distribution not only is directly affected by the prevalent mechanism but also has a great dependency on the acidity of the catalyst or its Si/Al ratio used in the synthesis of zeolite.[8] On the other hand, by changing the zeolite properties, this distribution may change completely. In turn, the different product distributions would lead to some minor or major modifications in the backbone of the kinetic scheme or may

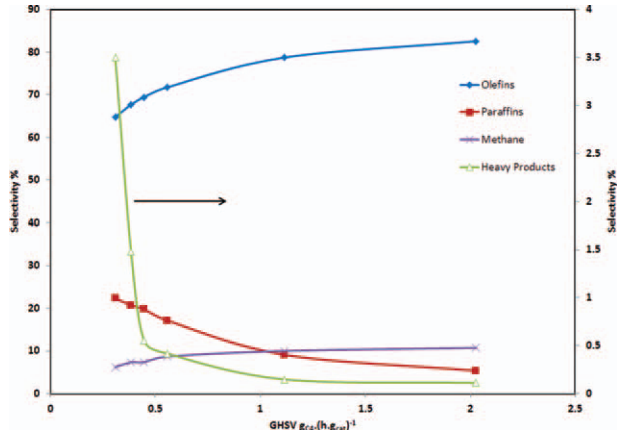

Figure 8. Effect of GHSV on product distribution from *i*-butane cracking at 530°C.

[Color figure can be viewed in the online issue, which is available at wileyonlinelibrary.com.]

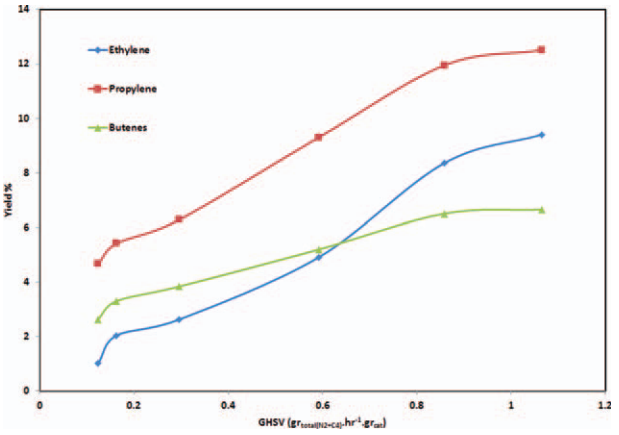

Figure 10. Variation of light olefin yield with contact time at 530°C.

[Color figure can be viewed in the online issue, which is available at wileyonlinelibrary.com.]

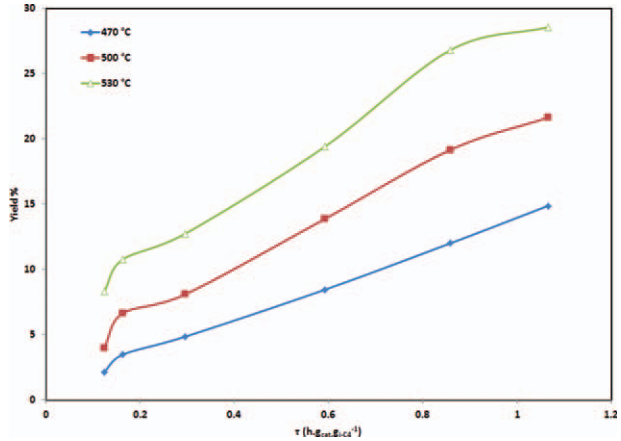

Figure 11. Effect of contact time on light olefin yields in *i*-butane cracking at different temperatures.

[Color figure can be viewed in the online issue, which is available at wileyonlinelibrary.com.]

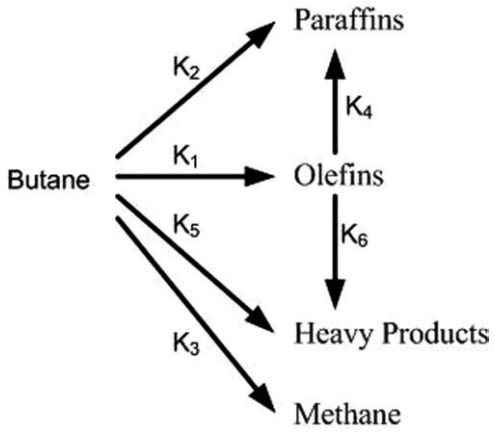

Figure 13. Kinetic scheme with five lumps: butane (*i*- or *n*-butane as reactant), olefins (ethylene, propylene, and butene), paraffins (ethane, propane, and *i*- or *n*-butane: isomer of the reactant), heavy products (C_5–C_7).

even necessitate a complete replacement of it. In general, to select or alter a kinetic scheme in the cracking reaction of paraffin gases over zeolites, the following items should be carefully considered:

A. Physical justifications and rationalizations for achieving a suitable kinetic scheme including
   1. Product distribution
   2. Acidity of the catalyst samples used
   3. Operating variables and
   4. Prevalent kinetic mechanism (monomolecular or bimolecular), which may be inferred from the items above (1–3)

B. Statistical justifications including
   1. Identifying all necessary statistical functions relating to determination of variance and parameters indicating significance of the model
   2. Calculating such parameters and rationalizing the obtained values

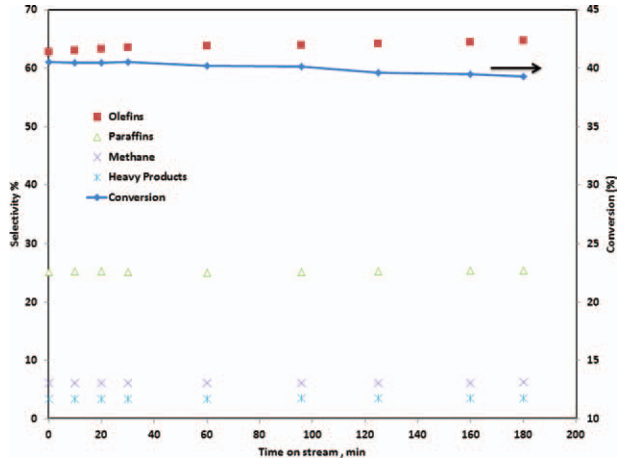

Figure 12. Evolution of feed conversion (right axis) and product selectivity (left axis) with time-on-stream, GHSV = 0.31 $g_{i\text{-}C_4}$ (h g_{cat})$^{-1}$, at T =530°C.

[Color figure can be viewed in the online issue, which is available at wileyonlinelibrary.com.]

Initially, the kinetic scheme provided by Mier et al.[2] was used in the present study; however, the results were not promising and that model's predictions did not fit the experimental data obtained in this research. Next, in spite of changing the reactions order of that scheme,[2] this disagreement was repeated. It was recognized that reasons for such disputes might have been due to different factors including acidity of the catalyst (Si/Al ratio), partial pressure of the feed, and also feed contact time between the present study and those of Mier et al. This led to the idea of the necessity to change the kinetic scheme.

Based on the aforementioned determinant factors and according to Table 2, which is derived from Nguyen et al.[21] work, important reactions were classified into the following categories.

Rows 1 and 2 in Table 2 are the characterization of the primary products based on the monomolecular mechanism and Rows 3 and 4 are the consequences of bimolecular mechanism. Therefore, Reactions 1 and 3 in the proposed kinetic scheme, Figure 13, might be rationalized to take place in the same category as those of Rows 1, 2, and 3 of Table 2, leading to methane and light olefins production according to the protolytic cracking (i.e., attack of zeolite active sites on C—H or C—C bond of butane) and bimolecular mechanism. Reactions 4 and 5 of the proposed kinetic scheme in the present model, however, might be explained through hydrogen transfer reactions due to Row 3 of the table. Reaction 6 in the kinetic scheme of the present study might be considered in the same category as that of Row 4 of the

Table 2. Different Reaction Categories for *i*-Butane and *n*-Butane Cracking over the HZSM-5 Zeolite

1	$C_4 \rightarrow C_4^{2-} + H_2$	Protolytic cracking C—H bond of butane over zeolite acid sites
2	$C_4 \rightarrow C_n^{2-} + C_{4-n}$	Protolytic cracking of C— C bond of butane over zeolite acid sites $2 \leq n$
3	$C_4 + C_n^{2-} \rightarrow C_4^{2-} + C_n$	Hydrogen transfer between butane and light or heavy olefins and formation of paraffins and butane
4	$C_n^{2-} + C_m^{2-} \rightarrow C_{n+m}^{2-}$	Olefin oligomerization $2 \leq n,m \leq 6$, $n + m \leq 8$

table. Ultimately, as paraffins are formed through combination of reactions in Rows 2 and 3 of the table, Reaction 2 in the present kinetic scheme was considered as a separate step to distinguish it from the olefin production and butane consumption steps, hence no interference with Reaction 1 or 4 occurred. This collective view yielded the presented kinetic scheme which took into account all aspects of both monomolecular and bimolecular mechanisms.

Ultimately, it should be reminded that, when the kinetic model describing a process becomes a lumped one, the kinetic scheme does not provide elementary reactions at every proposed step anymore. This is due to the fact that each step of the lumped model is now due to a group of several reactions possibly taking place from reactants under consideration. Thus, the order of the reaction with respect to such reactants is best determined by fitting of the experimental data. Hence, reaction orders and stoichiometry are not directly related to the lumped modeling. Nevertheless, the goodness of the fit with experimental data is the determining factor.

Estimation of Kinetic Parameters

Because the temperature difference along the bed was less than 1°C, the fixed-bed reactor was considered to be an isothermal plug flow reactor. The total reaction rate of each lump i, expressed by r_i, was calculated as the sum of all reaction rates at different steps in which lump i was involved

$$r_i = \frac{dX_i}{d(r)} = \sum_{j=1}^{n_r} (\nu_i)_j r_j \ \frac{(\mathrm{mol_i})\mathrm{CH_2}}{\mathrm{g.h}} \tag{6}$$

where

$$r = \frac{W}{F_o} \tag{7}$$

In Eqs. 6 and 7, X_i is the mole fraction of lump i in the reaction medium (based on CH_2 units), τ is the butane contact time in g_{cat} h $g_{Cr}{}^{-1}$, r_j is the rate of reaction step j, n_r is the number of reaction steps, and $(\nu_i)_j$ is the stoichiometric coefficient of lump i in reaction step j. To simplify the calculations, the mole fraction X_i in the rate equations was expressed as the molar fraction of lumped ion (CH_2 unit basis). By definition, X_i can be readily related to the partial pressure of the corresponding lump. Integration of the resulting set of differential equations was performed using the Adams–Bashforth–Moulton method and a program in MATLAB (R2010-a).[27] Kinetic parameters for the proposed model were estimated by minimizing the following error objective function, established as the sum of the squares of the differences between the experimental and calculated mole fraction of different lumps[28]

$$\mathrm{OF} = \sum_{i=1}^{n_l} \sum_{k=1}^{m} (X_{ik} - X_{ik}{}^{\mathrm{cal}})^2 \tag{8}$$

where n_l is the number of lumps, m is the number of experimental points excluding repetitions, $X_{ik}{}^{\mathrm{cal}}$ is the calculated mole fraction of lump i for experimental condition k, determined by solving the mass balance of Eq. 6 using a CH_2 basis (i.e., corresponding to a given value of contact time and temperature), and X_{ik} is the experimental mole fraction of lump i for experimental condition k. Estimated kinetic parameters were obtained by nonlinear regression using the Levenberg–Marquardt algorithm in MATLAB.[29] Kinetic parameters to be optimized included Arrhenius parameters for the rate constant for each reaction step j. To reduce the correlation between the frequency factor and activation energy, reparameterization was applied.[2,30–32] The Arrhenius equation of the rate constant was as follows

$$k_j = A_j \ \exp\left(-\frac{E_j}{RT}\right) \tag{9}$$

After introduction of the mean temperature, T_m, rate coefficients for the formation of primary products can be written

$$K_j = \exp\left[\left(\ln A_j - \frac{E_j}{RT_m}\right) - \frac{E_j}{R}\left(\frac{1}{T} - \frac{1}{T_m}\right)\right] \tag{10}$$

The expression for k_j thus becomes

$$K_j = K_j{}^* \ \exp\left[-\frac{E_j}{R}\left(\frac{1}{T} - \frac{1}{T_m}\right)\right] \tag{11}$$

Consequently, at $T_m = 500$°C, the parameters to be optimized are the kinetic constant at a reference temperature and the activation energy for each reaction step j.

To test the fit between the model and experimental points, a traditional statistical F-test was used to examine the significance of parameters in a regression model. This tes involved partitioning the sum of squares of residuals ($SS_{residual}$) into two components, "pure error" and "lack of fit"

$$\mathrm{SS_{residual}} = (\mathrm{SS_{pure\ error}}) + (\mathrm{SS_{lack\ of\ fit}}) \tag{12}$$

The sum of squares of pure error ($SS_{pure\ error}$) is the sum of squares of the differences between each experimental mole fraction and the average of all experimental mole fractions under the same operating condition. The sum of squares of lack of fit ($SS_{lack\ of\ fit}$) is the weighted sum of squares of the differences between the average of replications of the mole fraction for each lump i corresponding to the same operating condition and fitted mole fraction. The weight for each experimental point is simply the number of replications of the mole fraction for point j. The variance for the lack of fit and pure error is defined as the ratio of the sum of squares over the degrees of freedom. The degrees of freedom are the number of independent points available to estimate a parameter. Statistical functions and definitions for the degrees of freedom corresponding to those functions are provided elsewhere.[2,33,34] To evaluate the significance of the model, the variances of pure error and the lack of fit were compared. For this comparison, an F-ratio test statistic was calculated, which provides a measure of testing the null hypothesis or the statistical significance of the lack of fit, defined as the ratio of the variance of lack of fit over the variance of pure error

$$F = \frac{\sigma^2{}_{\mathrm{LF}}}{\sigma^2{}_{\mathrm{PE}}} \tag{13}$$

To verify that the kinetic model was appropriate, that lack of fit was not statistically significant, and that the null hypothesis was established, the test statistic value also had to satisfy the following expression

Table 3. Optimized Values of Kinetic Constants and Activation Energies for *n*-Butane Cracking

Reaction Step, j	k_j*	E_j (J mol^{-1})	Units for k_j*
1	$(8.50 \pm 1.41) \times 10^{-2}$	$(1.13 \pm 0.49) \times 10^{5}$	$mol_{CH_2}\ g_{cat}^{-1}\ h^{-1}\ (mol_{n\text{-}C_4}/mol)^{-2}$
2	$(5.66 \pm 2.01) \times 10^{-2}$	$(4.00 \pm 0.18) \times 10^{4}$	$mol_{CH_2}\ g_{cat}^{-1}\ h^{-1}\ (mol_{n\text{-}C_4}/mol)^{-1}$
3	$(7.20 \pm 0.74) \times 10^{-2}$	115 ± 2.00	$mol_{CH_2}\ g_{cat}^{-1}\ h^{-1}\ (mol_{n\text{-}C_4}/mol)^{-1}$
4	0.536 ± 0.211	155 ± 26.1	$mol_{CH_2}\ g_{cat}^{-1}\ h^{-1}\ (mol_{olefins}/mol)^{-2}$
5	$(2.30 \pm 0.728) \times 10^{-2}$	$(1.70 \pm 0.35) \times 10^{5}$	$mol_{CH_2}\ g_{cat}^{-1}\ h^{-1}\ (mol_{n\text{-}C_4}/mol)^{-1}$
6	$(4.00 \pm 2.30) \times 10^{-4}$	$(1.34 \pm 0.19) \times 10^{-4}$	$mol_{CH_2}\ g_{cat}^{-1}\ h^{-1}\ (mol_{olefins}/mol)^{-2}$

$$F < f(\alpha, \nu_{LF}, \nu_{PE}) \tag{14}$$

where $f(\alpha,\ \nu_{LF},\ \nu_{PE})$ is the critical value of the Fischer distribution function for given values of degrees of freedom, ν_{LF} and ν_{PE} and α is the significance level, usually 0.01 or 0.05. In the present case, a 95% confidence level (i.e., $100(1-\alpha)\%$) or $\alpha = 0.05$ was chosen. Critical values of the Fischer distribution function could be obtained from Fischer distribution tables,[35] or from the command $f_{inv}(100(1-\alpha),\ \nu_{LF}, \nu_{PE})$ included in MATLAB.

Modeling of n-*butane cracking*

Based on the kinetics scheme proposed in the section 5 and our *n*-butane cracking experimental data, chemical kinetics constants for the six reaction steps of this process were determined. Thus, assuming a second-order reaction for reaction steps involving olefins (i.e., regardless of whether the olefin was produced or consumed) and unity for other reaction steps resulted in the following rate expressions

$$r_{n-C_4} = -k_1 X_{n-C_4}{}^2 - k_2 X_{n-C_4} - k_3 X_{n-C_4} - k_5 X_{n-C_4} \tag{15}$$

$$r_{olefins} = k_1 X_{n-C_4}{}^2 - k_4 X_{olefins}{}^2 - k_6 X_{olefins}{}^2 \tag{16}$$

$$r_{methane} = k_3 X_{n-C_4} \tag{17}$$

$$r_{paraffins} = k_2 X_{n-C_4} + k_4 X_{olefins}{}^2 \tag{18}$$

$$r_{heavy\ products} = k_5 X_{n-C_4} + k_6 X_{olefins}{}^2 \tag{19}$$

The 95% confidence interval of the estimated parameters of the best fit including the kinetic constants at reference temperature T_m and activation energies for the six reaction steps are presented in Table 3.

Statistical parameters and variance analysis for the *n*-butane cracking kinetic model corresponding to the functions are given in Table 4.

Table 4. Values of Error Objective Function and Variance Analysis of the Kinetic Model for *n*-Butane Cracking

Statistical Variable	*n*-Butane	*i*-Butane
OF	0.0174	0.0118
M	24	18
n_l	5	5
SSLF	0.0106	0.0076
SS_{PE}	0.0064	0.0042
ν_{LF}	108	78
ν_{PE}	30	30
n_p	12	12
σ^2_{LF}	9.82×10^{-5}	9.74×10^{-5}
σ^2_{PE}	2.13×10^{-4}	1.4×10^{-4}
F	0.461	0.695
$f(\alpha,\nu_{LF}, \nu_{PE})$	1.690	1.714
Significance test	Valid	Valid

The predicted and experimental mole fractions of various lumps from the catalytic cracking of *n*-butane as a function of contact time are shown in Figures 14a, b for different reaction temperatures and indicate very satisfactory agreement between these values. Furthermore, the value of the objective function (see Eq. 8) was 0.0174, highlighting the accuracy of the present model. Finally, results of variance analysis indicate the validity of the proposed kinetic scheme.

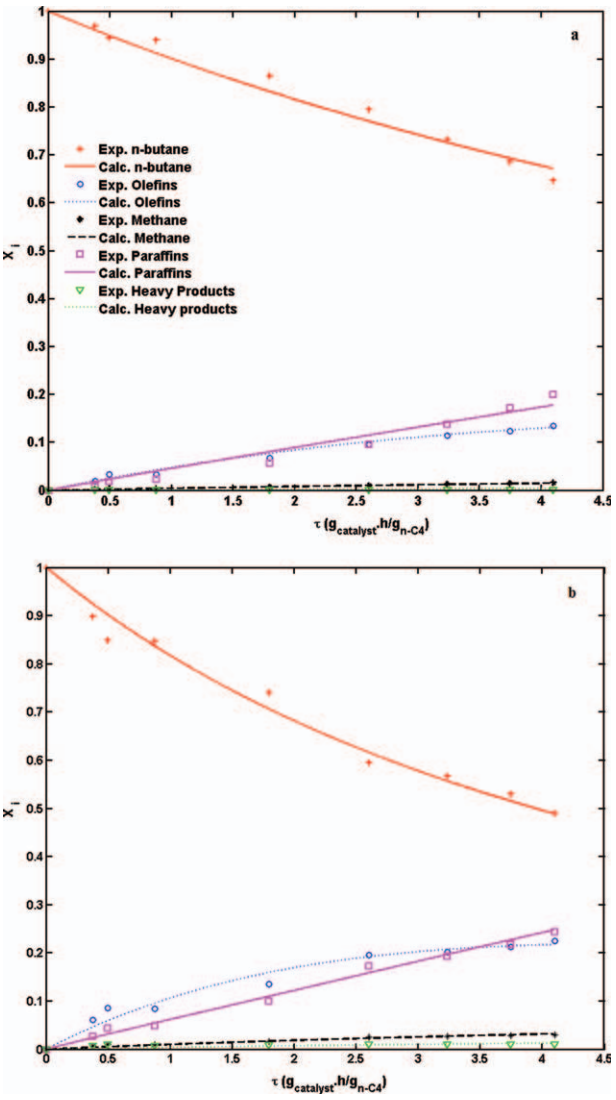

Figure 14. Comparison between the experimental data (depicted as symbols) and predicted values (depicted as lines) for *n*-butane cracking, partial pressure = 20 kPa: (a) 470°C and (b) 530°C.

[Color figure can be viewed in the online issue, which is available at wileyonlinelibrary.com.]

Table 5. Optimized Values of Kinetic Constants and Activation Energies for *i*-Butane Cracking

Reaction Step, j	k_j*	E_j (J mol^{-1})	Units for k_j*
1	0.101 ± 0.010	$(1.15 \pm 0.91) \times 10^5$	$mol_{CH_2}\ g_{cat}^{-1}\ h^{-1}\ (mol_{i\text{-}C_4}\ /\ mol)^{-2}$
2	$(3.03 \pm 1.39) \times 10^{-2}$	$(4.65 \pm 0.78) \times 10^4$	$mol_{CH_2}\ g_{cat}^{-1}\ h^{-1}\ (mol_{i\text{-}C_4}\ /\ mol)^{-1}$
3	$(8.20 \pm 2.29) \times 10^{-2}$	$(8.78 \pm 0.72) \times 10^4$	$mol_{CH_2}\ g_{cat}^{-1}\ h^{-1}\ (mol_{i\text{-}C_4}\ /\ mol)^{-1}$
4	0.223 ± 0.083	352 ± 181	$mol_{CH_2}\ g_{cat}^{-1}\ h^{-1}\ (mol_{olefins}\ /\ mol)^{-2}$
5	$(5.90 \pm 1.90) \times 10^{-2}$	49.2 ± 5.40	$mol_{CH_2}\ g_{cat}^{-1}\ h^{-1}\ (mol_{i\text{-}C_4}\ /\ mol)^{-1}$
6	$(6.00 \pm 4.00) \times 10^{-5}$	$(3.28 \pm 0.27) \times 10^4$	$mol_{CH_2}\ g_{cat}^{-1}\ h^{-1}\ (mol_{olefins}\ /\ mol)^{-2}$

Similar data at 500°C were obtained, reported as the supplementary data and might be obtained from the *AIChE Journal*.

Modeling of i*-butane cracking*

A similar approach to that used for *n*-butane cracking was used to model the kinetics of *i*-butane cracking. The following rate expressions were determined

$$r_{i-C_4} = -k_1 X_{i-C_4}^2 - k_2 X_{i-C_4} - k_3 X_{i-C_4} - k_5 X_{i-C_4} \quad (20)$$

$$r_{olefins} = k_1 X_{i-C_4}^2 - k_4 X_{olefins}^2 - k_6 X_{olefins}^2 \quad (21)$$

$$r_{methane} = k_3 X_{i-C_4} \quad (22)$$

$$r_{paraffins} = k_2 X_{i-C_4} + k_4 X_{olefins}^2 \quad (23)$$

$$r_{heavy\ products} = k_5 X_{i-C_4} + k_6 X_{olefins}^2 \quad (24)$$

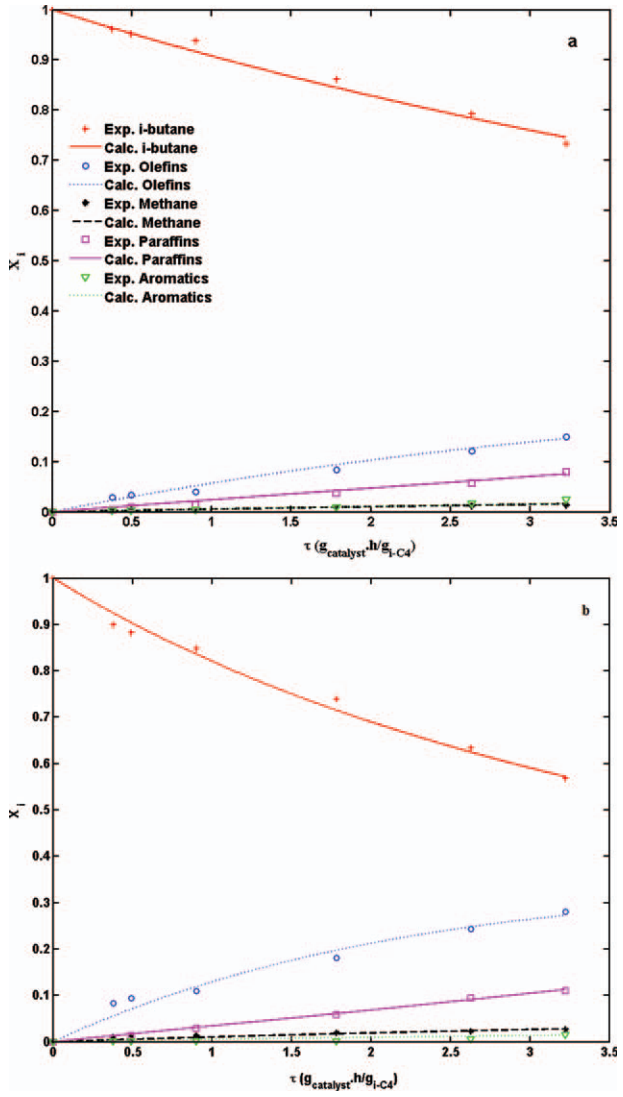

Figure 15. Comparison between the experimental data (depicted as symbols) and predicted values (depicted as lines) for *i*-butane cracking, partial pressure = 20 kPa: (a) 470°C and (b) 530°C.

[Color figure can be viewed in the online issue, which is available at wileyonlinelibrary.com.]

Table 5 shows the chemical kinetic constants and activation energies for the six reaction steps in *i*-butane cracking. Based on the results of variance analysis of the kinetic model for *i*-butane cracking (shown in Table 4), the validity of the model was confirmed by Fischer's test. The adequacy of the fit is illustrated in Figures 15a, b where the predicted and experimental mole fractions of various lumps for this process as a function of contact time are presented at different reaction temperatures, indicating very satisfactory agreement between these values.

Similar data at 500°C were obtained, reported as the supplementary data and might be obtained from the *AIChE Journal*.

Conclusion

An HZSM-5 zeolite with a high SiO_2/Al_2O_3 ratio was synthesized to obtain high selectivity toward light olefins during catalytic cracking of *n*-butane and *i*-butane. For both reactants, this catalyst displayed low selectivity for the production of heavy products, which may be due to the low aluminum content in the zeolite structure. Our results also indicate that selectivity toward light olefins increases with increasing temperature and decreasing contact time, whereas selectivity toward paraffins and heavy products decreases. A lumped kinetic model consisting of five lumps and six reaction steps is proposed, and the corresponding chemical kinetic parameters were estimated. The proposed model is simple, and yet accurately predicts product conversions and distributions from catalytic cracking of both reactants. Second-order reactions were found to be the best for reactions involving light olefin production or consumption, whereas first-order reactions were better for all other reactions. The agreement between experimental and predicted mole fractions of different lumps was very satisfactory for both reactants. Ultimately, this study paved down the roads for similar studies to be done toward the joint reaction of coupled methanol and paraffin into olefins.

Notation

A_j = frequency factor of Arrhenius equation for reaction j
d_p = average pore diameter, nm
E_j = activation energy for reaction j, kJ mol^{-1}
F = test statistics or F ratio, defined as ratio of variance of lack of fit over variance of pure error, Eq. 12

F_o = inlet butane molar flow rate, mol h^{-1}
F_e = outlet butane molar flow rate, mol h^{-1}
F_{ie} = exit molar flow rate of compound i, mol h^{-1}
$f(\alpha,\nu_{LF},\nu_{PE})$ = critical value of the Fischer distribution function for the given values of degrees of freedom and significance level, α
GHSV = gas hourly space velocity, g_{C_4} (h g_{cat})$^{-1}$
k_j, k_j* = kinetic constants for step j, at any temperature, and that corresponding to the reference temperature (units are those corresponding to the kinetic equation)
m = number of experimental points excluding the repetitions
n_i = number of carbon atoms for compound i
n_l = number of lumps
n_p = number of kinetic parameters to be optimized
OF = error objective function, Eq. 7
R = universal gas constant, kJ (mol K)$^{-1}$
R_j = number of repetitions under given experimental conditions
r_i = total reaction rate of lump i
r_j = reaction rate of step j in the kinetic scheme
S_{BET} = BET surface area, m^2 g^{-1}
SS_{LF}, SS_{PE} = sum of squares for the lack of fit and for pure experimental error
T, T_m = temperature and reference temperature, K
V_p = total pore volume, cm^3 g^{-1}
W = weight of the catalyst used, g
X_i = molar fraction of lump i, in CH_2 equivalent units
X_{ik} = experimental composition of lump i for the experimental condition k
$\overline{X}_{ij}$ = average composition of lump i determined from experiments repeated under the same experimental condition j
X_{ij}^{cal} = calculated composition of lump i for the experimental condition j

Greek letters

α = significance level
$(\upsilon_i)_j$ = stoichiometric coefficient of component i in step j in the kinetic scheme
τ = butane contact time, h g_{cat} $g_{C_4}^{-1}$
σ^2_{LF}, σ^2_{PE} = variances for the lack of fit of the kinetic model, and pure error
ν_{LF},ν_{PE} = degrees of freedom for the lack of fit and for pure error

Literature Cited

1. Caeiro G, Carvalho RH, Wang X, Lemos M, Lemos F, Guisnet M, Ribeiro FR. Activation of C_2–C_4 alkanes over acid and bifunctional zeolite catalysts. *J Mol Catal A: Chem*. 2006;255:131–158.
2. Mier D, Aguayo AT, Gayubo AG, Olazar M, Bilbao J. Kinetic modeling of *n*-butane cracking on HZSM-5 zeolite catalyst. *Ind Eng Chem Res*. 2010;49:8415–8423.
3. Mier D, Aguayo AT, Gayubo AG, Olazar M, Bilbao J. Synergies in the production of olefins by combined cracking of *n*-butane and methanol on a HZSM-5 zeolite catalyst. *Chem Eng J*. 2010;160: 760–769.
4. Mier D, Aguayo AT, Gayubo AG, Olazar M, Bilbao J. Catalyst discrimination for olefin production by coupled methanol/*n*-butane cracking. *Appl Catal A: Gen*. 2010;383:202–210.
5. Available at: http://www.uop.com/objects/10%20ARTCUOPOnPurposePropylene.pdf.
6. Ren T, Patel M, Blok K. Steam cracking and methane to olefins: energy use, CO_2 emissions and production costs. *Energy*. 2008;33:817–833.
7. Haag WO, Dessau RM. *Proceedings of the 8th International Congress of Catalysis*.Frankfurt-am-Main, 1984:305.
8. Corma A, Orchilles AV. Current views on the mechanism of catalytic cracking. *Microporous Mesoporous Mater*. 2000;35:21–30.
9. Wielers AFH, Vaarkamp M, Post MFM. Relation between properties and performance of zeolites in paraffin cracking. *J Catal*. 1991;127:51–66.
10. Corma A, Miguel PJ, Orchilles AV. The role of reaction temperature and cracking catalyst characteristics in determining the relative rates of protolytic cracking, chain propagation, and hydrogen transfer. *J Catal*. 1994;145:171–180.
11. Narbeshuber TF, Brait A, Seshan K, Lercher JA. Dehydrogenation of light alkanes over zeolites. *J Catal*. 1997;172:127–136.
12. Haag WO, Lago RM, Weisz PB. Transport and reactivity of hydrocarbon molecules in a shape-selective zeolite. *Farad Discuss Chem Soc*. 1981;72:317–330.
13. Collins SJ, O'Malley PJ. A theoretical description for the monomolecular cracking of C—C bonds over acidic zeolites. *J Catal*. 1995;153:94–99.
14. Krannila H, Haag WO, Gates BC. Monomolecular and bimolecular mechanisms of paraffin cracking: *n*-butane cracking catalyzed by HZSM-5. *J Catal*. 1992;135:115–124.
15. Shigeishi R, Garforth A, Harris I, Dwyer J. The conversion of butanes in HZSM-5. *J Catal*. 1991;130:423–439.
16. Narbeshuber TF, Vinek H, Lercher JA. Monomolecular conversion of light alkanes over H-ZSM-5. *J Catal*. 1995;157:388–395.
17. Ono Y, Kanae K. Transformation of butanes over ZSM-5 zeolites. *J Chem Soc Faraday Trans*. 1991;87:663–667.
18. Bizreh YW, Gates BC. Butane cracking catalyzed by the zeolite H-ZSM-5. *J Catal*. 1984;88:240–243.
19. Wakui K, Satoh K, Sawada G. Cracking of *n*-butane over alkaline earth-containing HZSM-5 catalysts. *Catal Lett*. 2002;84:259–264.
20. Wakui K, Satoh K, Sawada G, Shiozawa K, Matano K, Suzukiu K, Hayakawa T, Yoshimura Y, Murata K, Mizukami F. Dehydrogenerative cracking of *n*-butane using double-stage reaction. *Appl Catal A: Gen*. 2002;230:195–202.
21. Nguyen LH, Vazhnova T, Kolaczkowski ST, Lukyanov DB. Combined experimental and kinetic modeling studies of the pathways of propane and *n*-butane aromatization over H-ZSM-5 catalyst. *Chem Eng Sci*. 2006;61:5881–5894.
22. Pinto RR, Borges P, Lemos A, Lemos F, Ribeiro FR. Kinetic modeling of the catalytic cracking of *n*-hexane and *n*-heptane over a zeolite catalyst. *Appl Catal A: Gen*. 2004;272:23–28.
23. Lukyanov DB, Gnep NS, Guisnet MS. Kinetic modeling of ethene and propene aromatization over HZSM-5 and GaHZSM-5. *Ind Eng Chem Res*. 1994;33:223–234.
24. Lukyanov DB, Gnep NS, Guisnet MS. Kinetic modeling of propane aromatization reaction over HZSM-5 and GaHZSM-5. *Ind Eng Chem Res*. 1995;34:516–523.
25. Lukyanov DB. Development of kinetic models for reactions of light hydrocarbons over ZSM-5 catalysts. Experimental studies and kinetic modelling of ethene transformation and deactivation of HZSM-5 catalyst. *Stud Surf Sci Catal*. 1999;122:299–306.
26. Lukyanov DB. Application of a kinetic model for investigation of aromatization reactions of light paraffins and olefins over HZSM-5. *Stud Surf Sci Catal*. 1997;105:1301–1308.
27. Shampine LF, Gordon MK. *Computer Solution of Ordinary Differential Equations: The Initial Value Problem*.San Francisco: W. H. Freeman and Company, 1975.
28. Gayubo AG, Alonso A, Valle B, Aguayo AT, Bilbao J. Deactivation kinetics of a HZSM-5 zeolite catalyst treated with alkali for the transformation of bio-ethanol into hydrocarbons. *AIChE J*. In press.
29. Marquardt FW. An algorithm for least-squares estimation of nonlinear parameters. *J Soc Ind Appl Math*. 1963;11:431–441.
30. Mier D, Aguayo AT, Gamero M, Gayubo AG, Bilbao J. Olefin production by co-feeding methanol and *n*-butane: kinetic modeling considering the deactivation of HZSM-5 zeolite. *AIChE J*. In press.
31. Kittrell JR, Mezaki R, Watson CC. Estimation of parameters for nonlinear least squares analysis. *Ind Eng Chem*. 1965;57:18–27.
32. Agarwal AK, Brisk ML. Sequential experimental design for precise parameter estimation. 1. Use of re-parameterization. *Ind Eng Chem Process Des Dev*. 1985;24:203–207.
33. Brook RJ, Arnold GC. *Applied Regression Analysis and Experimental Design*, 1st ed. London: CRC Press LLC Chapman & Hall, 1985:48–49.
34. Montgomery DC, Runger GC. *Applied Statistics and Probability for Engineers*, 3rd ed. New York: John Wiley & Sons, Inc., 2002.
35. Zwillinger D, Kokoska S. *CRC Standard Probability and Statistics Tables and Formulae*. London: CRC Press LLC Chapman & Hall, 2000.

Manuscript received Apr. 12, 2011, and revision received July 23, 2011.